The Coulomb critical taper theory applied to gravitational instabilities

Régis Mourgues, Aurélien Lacoste, Cynthia Garibaldi

▶ **To cite this version:**

Régis Mourgues, Aurélien Lacoste, Cynthia Garibaldi. The Coulomb critical taper theory applied to gravitational instabilities. Journal of Geophysical Research : Solid Earth, 2014, 119 (1), pp.754–765. 10.1002/2013JB010359 . hal-02377298

HAL Id: hal-02377298
https://hal.science/hal-02377298

Submitted on 8 Jul 2021

HAL is a multi-disciplinary open access archive for the deposit and dissemination of scientific research documents, whether they are published or not. The documents may come from teaching and research institutions in France or abroad, or from public or private research centers.

L'archive ouverte pluridisciplinaire **HAL**, est destinée au dépôt et à la diffusion de documents scientifiques de niveau recherche, publiés ou non, émanant des établissements d'enseignement et de recherche français ou étrangers, des laboratoires publics ou privés.

Copyright

AGU PUBLICATIONS

JGR

Journal of Geophysical Research: Solid Earth

RESEARCH ARTICLE
10.1002/2013JB010359

Key Points:
- We apply the critical taper theory to gravity instabilities
- We provide an alternative exact solution better suited to slope instabilities
- We verify the theory with scaled experiments involving pore fluid

Correspondence to:
R. Mourgues,
Regis.Mourgues@univ-lemans.fr

Citation:
Mourgues, R., A. Lacoste, and C. Garibaldi (2014), The Coulomb critical taper theory applied to gravitational instabilities, *J. Geophys. Res. Solid Earth*, *119*, 754–765, doi:10.1002/2013JB010359.

Received 15 MAY 2013
Accepted 10 DEC 2013
Accepted article online 17 DEC 2013
Published online 29 JAN 2014

The Coulomb critical taper theory applied to gravitational instabilities

R. Mourgues[1], A. Lacoste[2], and C. Garibaldi[1]

[1]LUNAM, L.P.G.N., UMR 6112, Faculty of Science, Université du Maine, Le Mans, France, [2]GeHCO, E.A.6293, Université de Tours, Tours, France

Abstract The critical Coulomb wedge theory has been widely applied to the structural evolution of accretionary wedges and fold and thrust belts, but it also predicts the spreading of a wedge under gravity. This solution may be applied to the formation of gravitational spreading and gliding along passive margins, where elevated pore fluid pressure is common. Following the initial hypotheses of the theory, we provide an alternative expression of the exact solution for a noncohesive wedge, better suited to slope instabilities. Our formulation allows a direct calculation of the fluid pressure required for the system to deform and predicts two kinds of gravitational deformation: shallow slumping and/or deep gravitational spreading rooting on the basal detachment. To verify the predictions of the model, we performed scaled experiments with pore pressure under conditions close to the critical taper hypotheses. The good agreement between our experimental results and the theory confirms the applicability of the critical taper model to the formation of gravitational structures in sedimentary wedges subjected to pore fluid pressure.

1. Introduction

The understanding of the evolution of deformation is a key issue in analyzing geological processes, such as orogenic episodes or the triggering of gravitational instabilities. In a series of influential papers dealing with analyses of the mechanics of fold and thrust belts and accretionary prisms, *Davis et al.* [1983], *Dahlen et al.* [1984], and *Dahlen* [1984, 1990] showed that the mechanical and structural evolution of wedge-shaped masses deforming above a detachment plane could be described by the critical Coulomb wedge theory. *Davis et al.* [1983] compared the evolution of a submarine accretionary wedge to that of a pile of sand in front of a moving bulldozer. The wedge steepens until the critical taper is attained, i.e., the angle between the base and the surface of the wedge reaches a critical value. When the critical taper is attained, the wedge is considered to be stable: Deformation is restricted to sliding along the detachment plane. *Dahlen* [1984] provided an exact general solution to the problem of the critical taper of noncohesive wedges. His formulation has multiple solutions, depending on the shear orientation on the basal detachment and the state of stress (i.e., compressive or extensional, respectively) within the wedge (Figure 1).

The good agreement between the analytical solution applicable to systems subjected to compressive forces (where the basal shear stress is directed toward the outer edge of the wedge, Figure 1) and natural examples, such as the accretionary prisms of Taiwan [*Suppe*, 1981, 2007] or the Barbados [*Zhao et al.*, 1986; *Kopf and Brown*, 2003], has been widely supported by experimental and numerical data [e.g., *Davis et al.*, 1983; *Mulugeta*, 1988; *Willett*, 1992; *Lallemand et al.*, 1994; *Martinez et al.*, 2002; *Simpson*, 2011]. However, though pore fluid pressure is a key parameter having a strong influence on both the strength of the wedge and the basal sliding resistance [e.g., *Terzaghi*, 1923; *Hubbert and Rubey*, 1959; *Lambe and Whitman*, 1969], most of these works neglected the influence of such pore pressure. The theoretical predictions for overpressured wedges have only been recently experimentally confirmed [*Pons and Mourgues*, 2012].

The case where the basal shear stress is oriented toward the inner part of the wedge (Figure 1) was termed as "extensional wedge" [*Xiao et al.*, 1991]. This critical taper solution describes the deformation of a wedge-shaped crust overlying a low-angle normal fault. Therefore, "extensional wedges" are found in active extensional settings. However, extensional states of stress are not restricted to such regime. Effectively, in the absence of any compressive or extensional force, the shear stress at the base is oriented toward the outer edge of the wedge (Figure 1). In that case, the critical taper corresponds to the maximal surface slope sustainable by the wedge before it slides under its own weight. On one hand, this process was clearly initially identified by *Dahlen* [1984],

©2013. American Geophysical Union. All Rights Reserved.

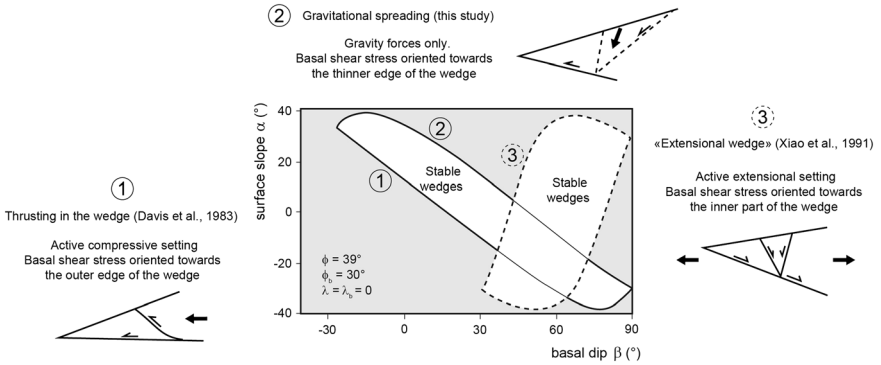

Figure 1. Synthetic diagram showing critical taper solutions for extensional and compressive dry sand wedges. Solid line indicates stability boundaries of systems where the basal shear stress is oriented toward the outer edge of the wedge (cases of sketch 1, *Davis et al*. [1983] and sketch 2, this study). Dashed line indicates stability boundaries of systems where the basal shear stress is oriented toward the inner part of the wedge (case of sketch 3, modified after *Xiao et al*. [1991]).

and it has been extensively applied to the study of gravitational spreading in orogenic wedges deforming above a viscous crust [e.g., *Platt*, 1986] and accretionary wedges subjected to large-scale underplating [*Lallemand et al*., 1994; *Gutscher et al*., 1998; *Kukowski et al*., 2001]. On the other hand, few studies focused on the applicability of this solution to gravitational spreading and gliding along passive margins, where elevated pore fluid pressure is common in sediments and where numerous gravitational structures, such as landslides and debris flows, are identified (e.g., Storegga slide, Norway [*Kvalstad et al*., 2005] and Demerara Rise, French Guiana [*Pattier et al*., 2011]).

The fold and thrust belts constituting the downslope part of large-scale submarine systems gravitationally detaching on salt layers or overpressured shale (up to a hundred kilometers wide) (e.g., Niger delta [*Bilotti and Shaw*, 2005] and Amazon fan [*Reis et al*., 2010; *Morley et al*., 2011]) have been compared to the orogenic contractional structures described in critical taper studies. Nevertheless, these authors limited their analyses to the compressive edge and did not carry out further investigations on the extensional upslope part of the system. Moreover, submarine slope instabilities are generally studied at a local scale, using simplified 1-D infinite slope analysis [*Mello and Pratson*, 1999], 2-D slices method [*Bishop*, 1955; *Lambe and Whitman*, 1969], two-wedge models [*Lambe and Whitman*, 1969; *Nadim et al*., 2003; *Leynaud et al*., 2004], or numerical simulations [*Hutton and Syvitski*, 2004]. *Kukowski et al*. [2010] also investigated the stability of slopes along the Hikurangi margin of New Zealand using a critical taper analysis. Nonetheless, the applicability of the critical Coulomb wedge theory to the case of gravity-driven extension has not yet been supported by further experimental or numerical studies. To our knowledge, only *Morgan and McGovern* [2005] compared the critical taper solution in the extensional part of a volcanic system subjected to gravitational collapse with numerical simulations (discrete element method). However, their analysis did not take into account the role of pore fluid pressure on deformation.

In this article, we investigate the applicability of the critical Coulomb wedge theory to gravitational instabilities. We limit our analysis to systems subjected to pore fluid pressure, in the absence of any external compressive or extensional forces. We briefly review the theory and propose an alternative expression of *Dahlen's* [1984] solution, better suited to the study of slope instabilities. To validate the predictions of this analytical model, we also document a series of physical experiments in which compressed air was applied at the base of dry sand wedges to trigger gravitational instabilities [*Mourgues and Cobbold*, 2006a, 2006b; *Lacoste et al*., 2012].

2. Expression of the Coulomb Wedge Theory in the Case of Gravitational Spreading

The complete developments of the critical Coulomb wedge theory are found in a series of paper by *Davis et al*. [1983], *Dahlen et al*. [1984], and *Dahlen* [1984, 1990]. Following the initial hypotheses of this theory, hereafter summarized, an alternative expression of the solution, better suited to slope instabilities, is provided.

The critical taper theory is based on the assumption that the internal state of stress of a wedge composed of material deforming following the Mohr-Coulomb criterion is on the verge of failure everywhere [*Davis et al*., 1983]. The shape of the wedge, growing self-similarly, depends on the strength of the material and on the relative magnitude of the resistance to sliding at the base. Let α denote the angle of the planar surface slope

©2013. American Geophysical Union. All Rights Reserved.

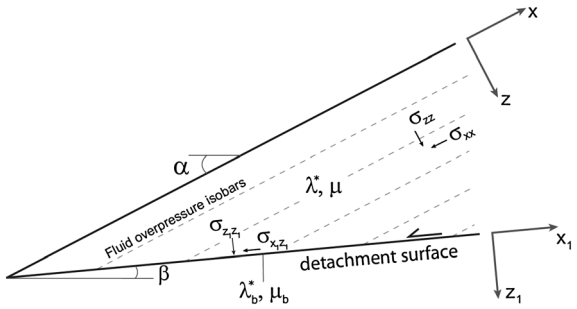

Figure 2. Schematic cross section of a wedge subjected to pore fluid pressure, parameters, and coordinate systems used in this study.

and β the dip of the basal décollement of a triangular submarine wedge (Figure 2). Values of α and β are positive where the surface slope and the basal detachment dip in the same direction. The static equilibrium of effective stresses in the system of Cartesian coordinates *x,z* (Figure 2) is

$$\frac{\partial \sigma'_{xx}}{\partial x} + \frac{\partial \sigma'_{xz}}{\partial z} = \rho' g \sin(\alpha) - \frac{\partial P_{ov}}{\partial x} \tag{1a}$$

$$\frac{\partial \sigma'_{xz}}{\partial x} + \frac{\partial \sigma'_{zz}}{\partial z} = \rho' g \cos(\alpha) - \frac{\partial P_{ov}}{\partial z} \tag{1b}$$

where g is the constant acceleration of gravity, σ' is the effective stress, ρ' the effective density (i.e., the density corrected from hydrostatic buoyancy), and P_{ov} the fluid overpressure (i.e., the pore fluid pressure exceeding the hydrostatic pressure) [*Hubbert and Rubey*, 1959]. The boundary conditions on the upper surface of the wedge ($z = 0$) are

$$\sigma'_{xz} = \sigma'_{zz} = 0 \tag{2}$$

Dahlen [1984] argued that if the wedge is uniform and noncohesive, the directions of stresses do not vary from place to place within the wedge. In that case, an exact treatment is possible, equations (1a), (1b), and (2) being satisfied by

$$\sigma'_{zz} = (1 - \lambda^*)\rho g z \cos(\alpha) \tag{3a}$$

$$\sigma'_{xz} = \rho g z \sin(\alpha) \tag{3b}$$

where λ^* is the fluid overpressure ratio [*Shi and Wang*, 1988; *Saffer and Bekins*, 1998] within the wedge

$$\lambda^* = P_{ov}/\rho g z \cos(\alpha) \tag{4}$$

Abnormal fluid pressures are indicated with λ^*. This coefficient is slightly modified from the generalized pore pressure ratio λ [*Hubbert and Rubey*, 1959; *Davis et al.*, 1983]. Effectively, in hydrostatic fluid pressure conditions, $\lambda \sim 0.4$, whereas $\lambda^* = 0$. In the following analysis, we use λ^*, more convenient to set as a boundary condition. Along submarine slopes, the upper sedimentary cover, saturated with water, may be subjected to strong compaction. In low-permeability sediments, the expulsion of water is slow, so that fluid pressure builds up to high values, close to those of the lithostatic pressure. This process, known as disequilibrium compaction, causes the pore fluid pressure to increase with depth. Though it might be more complex in natural systems, it is reasonable to assume as a first approximation that the pressure increase with depth is linear (hypothesis followed by Dahlen in the initial critical taper theory). Therefore, we assume that the fluid overpressure ratio λ^*, dependent on the fluid pressure and the lithostatic pressure, is kept constant within the wedge.

Equations (3a) and (3b) are conventionally used in one-dimensional infinite slope soil mechanics analyses [*Terzaghi*, 1943; *Jaeger and Cook*, 1979]. The determination of normal and shear stresses acting on the basal detachment requires the formulation of σ'_{xx}, which remains indefinite from equations (3a) and (3b). Let us consider the wedge on the verge of failure. Two distinct values of σ'_{xx} correspond to the extensional (upslope) and compressive (downslope) states of stress within such wedge, respectively. From geometrical considerations (see Appendix A):

$$\sigma'_{xx} = (2Y - 1)\sigma'_{zz} \tag{5}$$

©2013. American Geophysical Union. All Rights Reserved.

with

$$Y = \frac{1 - \sin(\phi)\sqrt{1 - FS^2}}{\cos^2(\phi)} \quad \text{in the extensional domain} \tag{6a}$$

$$Y = \frac{1 + \sin(\phi)\sqrt{1 - FS^2}}{\cos^2(\phi)} \quad \text{in the contractional domain} \tag{6b}$$

and

$$FS = \frac{\tan(\alpha)}{(1 - \lambda^*)\tan(\phi)} \tag{7}$$

where the detachment surface form parallel to the surface slope and ϕ is the angle of internal friction of the material. If the factor of safety FS = 1, the surface slope of the cover becomes unstable, thus triggering shallow landsliding. Note that Y cannot be calculated where FS > 1. Where the fluid pressure is in hydrostatic equilibrium ($\lambda^* = 0$), the maximum surface slope angle of the cover is the angle of repose of the material: $\alpha = \phi$. Where the wedge is subjected to fluid overpressure, the critical surface slope is reduced and is given by *Hubbert and Rubey* [1959] equation:

$$\tan\alpha = (1 - \lambda^*)\tan\phi \tag{8}$$

For the wedge to slide on a detachment not parallel to the surface, one has to consider a basal weak plane, defined by its own internal friction μ_b and fluid overpressure ratio λ^*_b:

$$\mu_b(1 - \lambda^*_b) < \mu(1 - \lambda^*) \tag{9}$$

where μ is the coefficient of internal friction of the material $\mu = \tan\varphi$. The introduction of two distinct parameters λ^* and λ^*_b implies that a sudden change of pore pressure occurs across the basal décollement, as is often observed across low-permeability sediments acting as seals for rising fluids (Figure 2) [*Osborne and Swarbrick*, 1997]. Therefore, the dependence of the value of λ^* on that of λ^*_b has to been taken into account. *Dahlen* [1984] defined the basal effective friction:

$$\mu'_b = \mu_b \frac{1 - \lambda_b}{1 - \lambda} \tag{10}$$

Consequently, the basal Coulomb boundary condition is written as

$$\tau_b = \mu'_b \sigma'_n \tag{11}$$

where τ_b is the basal shear stress within the detachment and σ'_n is the effective stress within the wedge, just above the basal detachment. The normal stress (σ'_n) and the shear stress (τ) acting on the detachment of the wedge are deduced from σ'_{xx}, σ'_{xz}, and σ'_{zz} by a change of Cartesian coordinates (x_1,z_1, Figure 2; see Appendix B) [*Jaeger and Cook*, 1979]:

$$\sigma'_n = E_1 \rho g z \cos(\alpha) \tag{12a}$$

$$\tau = E_2 \rho g z \cos(\alpha) \tag{12b}$$

With

$$E_1 = (1 - \lambda^*)\{Y + (1 - Y)\cos[2(\alpha - \beta)]\} + \tan(\alpha)\sin[2(\alpha - \beta)] \tag{13a}$$

$$E_2 = (1 - \lambda^*)\{(Y - 1)\sin[2(\alpha - \beta)]\} + \tan(\alpha)\cos[2(\alpha - \beta)] \tag{13b}$$

By substituting equations (12a) and (12b) into boundary condition 11, we express the fluid overpressure ratio required for the wedge to slide on a basal low-resistance layer as

$$\lambda^*_b = 1 - (1 - \lambda^*)\frac{E_2}{\mu_b E_1} \tag{14}$$

Though equation (14) is an alternative formulation of Dahlen's expression [*Dahlen*, 1984] and Lehner's graphical solution [*Lehner*, 1986], it allows a direct calculation of the fluid pressure (or the basal friction) required for sliding on the basal detachment, whereas Dahlen's critical taper exact solution required the resolution of an equation

©2013. American Geophysical Union. All Rights Reserved.

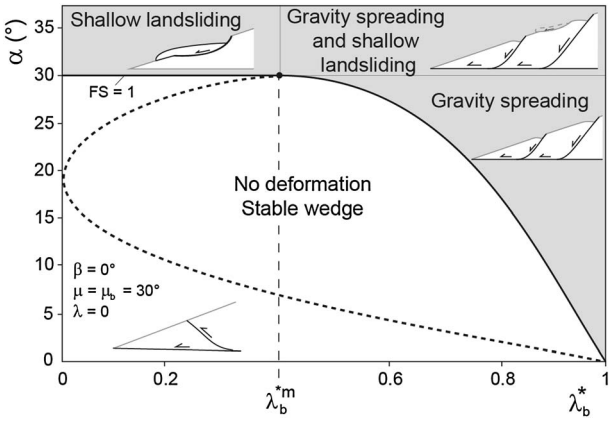

Figure 3. Critical taper solutions given by equation (14). The dashed line represents the solution for a compressive state of stress. The black bold line represents the solution for a gravity-driven extensional state of stress. The grey area shows domains of slope instability triggered by gravity only.

[*Dahlen*, 1984, equation (17)]. Equation (14) also provides important indications on the stability of the surface slope and the potential triggering of shallow slumps through the expression of the factor of safety FS (equation (7)).

Several domains are identified when plotting the solutions as a function of λ^*_b (Figure 3).

1. The central area shows surface slope angle and basal fluid overpressure ratio combinations for which the wedge remains stable, i.e., endures no internal plastic deformation.
2. The lower limit of this stable domain (dashed line, Figure 3) is valid in the case of a compressive state of stress. Below this limit, a wedge is considered to be subcritical and unstable (Figure 1). In such case, as insufficient shear stress is generated at the base to activate a basal detachment, the formation of thrust faults causes the wedge to steepen until it reaches its critical taper.
3. The upper limit of the stable domain corresponds to the critical surface slope of the wedge. The dashed part of this limit (Figure 3) is valid only for wedges subjected to compressive forces, whereas the black solid line corresponds to an extensional state of stress. Above this upper extensional limit, the wedge is predicted to thin, subside by gravity spreading, and deform by normal faulting.

In the case of thrusting under compressive forces, it is implicitly assumed that a sufficient force is applied to the system to initiate deformation. In the case of gravitational processes, sliding along a low-resistance detachment plane can be triggered as soon as the gravitational potential of the system is great enough to overcome the basal frictional resistance. Therefore, the upper extensional limit (Figure 3) is valid for active accretionary and orogenic wedges as well as for any passive margin slope subjected to gravity forces only. Gravitational spreading only requires the detachment surface to be subjected to a minimal pore fluid pressure ($\lambda^*{}_b{}^m$; Figure 3). Where $\lambda^*{}_b < \lambda^*{}_b{}^m$, sliding is restricted to shallow slumps (not rooting on the basal detachment surface), the critical slope being driven by the angle of repose of the surface (FS = 1; Figure 3).

3. Expression of the Basal Effective Friction

Dahlen [1984] justified the use of the effective coefficient of basal friction μ'_b (equation (10)) by expressing the basal shear stress condition, for a material obeying a Mohr-Coulomb criterion:

$$\tau_b = \mu_b(\sigma_n - P_b) = \mu'_b(\sigma_n - P) \tag{15}$$

where σ_n is the total normal stress acting on the detachment. P_b and P are the values of the pore pressure on the detachment surface and just above, respectively. On one hand, μ'_b (equation (10)) can be deduced from equation (15) by substituting the pore pressure P by a pore pressure ratio λ defined with respect to the normal stress σ_n acting on the detachment (expressed in the x_1,z_1 coordinate system, Figure 2) [*Davis et al.*, 1983]. On the other hand, *Dahlen* [1984] defined the coefficient of fluid pressure λ as a function of σ_{zz}, with respect to the x,z coordinate system, linked to the surface slope (equation (4) and Figure 2). This difference in the reference coordinate systems causes issues to arise [*Wang et al.*, 2006]. Indeed, according to equation (3a), and assuming uniform fluid overpressure ratios λ and λ_b, the total stress σ_{zz} is parallel to fluid pressure gradients (Figure 2) and therefore remains constant, regardless of the pore fluid overpressure [*Mourgues and Cobbold*,

©2013. American Geophysical Union. All Rights Reserved.

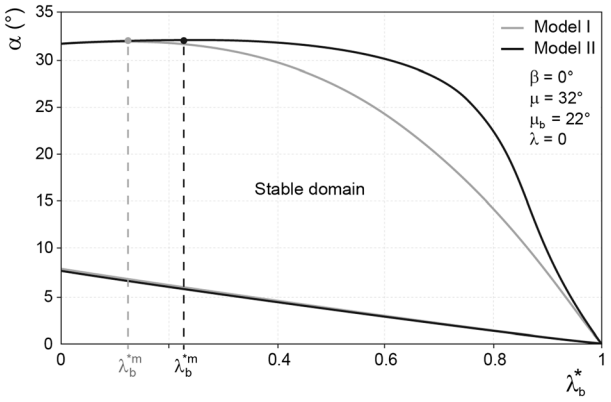

Figure 4. Critical taper solutions given by model I (grey solid line) and model II (black solid line) equations.

2003]. However, the total stress normal to the detachment (σ_{z1z1}, Figure 2) directly depends on the pore pressure [*Mourgues and Cobbold*, 2003]. Hence, to be consistent with the definition of λ used by *Dahlen* [1984], μ'_b should be expressed in the x_1,z_1 coordinate system. The shear stress on the basal detachment can then be written

$$\tau_b = \mu_b(\sigma_n - P_b) = \mu_b(\sigma'_n + P - P_b) = \mu_b(E_1 + \lambda^* - \lambda^*{}_b)\rho g z \cos(\alpha) = \mu'_b \sigma'_n = \mu'_b E_1 \rho g z \cos(\alpha) \quad (16)$$

where σ_n and σ'_n are the total and effective stresses acting within the wedge just above the basal detachment, respectively.

The effective coefficient of basal friction becomes

$$\mu'_b = \mu_b\left(1 + \frac{\lambda^* - \lambda^*{}_b}{E_1}\right) \quad (17)$$

Combining equations (16) and (12b), the fluid overpressure ratio required to trigger gravitational instabilities is expressed as

$$\lambda^*{}_b = E_1 + \lambda^* - \frac{E_2}{\mu_b} \quad (18)$$

Differences in the critical fluid overpressure ratio required to trigger sliding, as calculated using the basal effective friction given by *Dahlen* [1984] (equation (10)), hereafter denominated as model I, and the corrected basal effective friction given in equation (17) (model II), are illustrated in Figure 4. As observed by *Wang et al.* [2006],

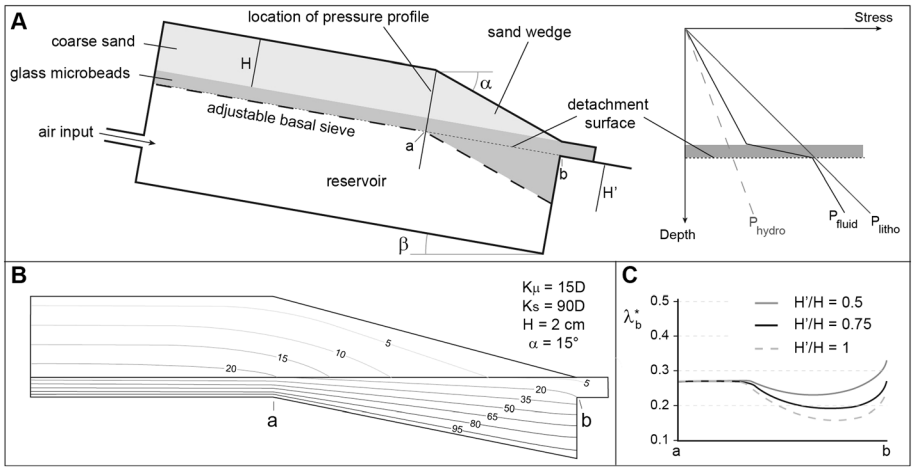

Figure 5. Experimental setup. (a) Schematic cross-section view (left) and pressure profile (right) along a wedge section perpendicular to the detachment surface. P_{hydro}: hydrostatic pressure; P_{fluid}: air pressure; P_{litho}: lithostatic pressure. (b) Cross-section view of pressure isobars (Pa), with K_μ the permeability of the glass microbeads (darcy) and K_s the permeability of the sand cover (darcy). (c) Coefficient of fluid pressure along the detachment surface, calculated for various values of H'.

©2013. American Geophysical Union. All Rights Reserved.

Table 1. Physical Properties of the Materials

Material	Grain Size (μm)	Bulk Density (kg m^{-3})	Angle of Internal Friction (°)	Coefficient of Internal Friction μ	Permeability (Darcy)
Coarse sand (cover)	300–400	1600	31	0.6	90
Glass microbeads (decollement)	200–300	1600	22	0.4	15

where the state of stress is compressive and critical taper angles are small (small angle approximation and lower limit of the stable domain, Figures 3 and 4), changes in the definition of the fluid overpressure ratio are negligible (Figure 4). Nevertheless, where such angles are greater (upper limit of the stable domain, Figures 3 and 4), the differences between model I and model II become significant. The minimal coefficient of fluid pressure required to trigger gravitational spreading instead of shallow slumping ($\lambda^*_b{}^m$, Figure 3) is slightly greater for model II (Figure 4). For a given surface slope angle, the destabilizing fluid pressure is also greater in model II. Moreover, the domain where the deformation is predicted to be dominated by gravitational spreading is reduced in model II, the critical surface slope angle being greater, for a given value of λ^*_b, than in model I.

4. Experimental Modeling

4.1. Experimental Setup and Procedure

We built an experimental setup in which compressed air was injected at the base of sand models (Figure 5a) [*Mourgues and Cobbold*, 2006a, 2006b; *Mourgues et al*., 2009; *Lacoste et al*., 2011, 2012]. The models were built on a 60 cm long and 40 cm large sieve and comprised a 0.5 cm thick basal low-permeability glass microbeads layer overlain by a coarse sand cover (thickness H, Figure 5a). The downslope edge of the cover had the shape of a triangular wedge. The surface slope of this wedge varied between 8° and 20°, depending on the series of experiments. We used materials having a negligible cohesion [*Schellart*, 2000], corresponding to the assumptions of the analytical model. The high permeability contrast between the glass microbeads and the sand (Table 1) allowed for fluid overpressure on the detachment surface (Figure 5a) [*Mourgues and Cobbold*, 2006a, 2006b]. Fluid pressure in the reservoir was monitored during the experiments using a U-manometer. We controlled the distribution of the coefficient of fluid pressure on the detachment surface by adjusting the dip of the sieve under the downslope edge (Figure 5a). Indeed, for λ^*_b to be constant along the detachment surface, the air pressure loss within the triangular edge of the model (Figure 5b) had to be balanced by adding glass microbeads underneath (thickness H′, Figure 5a) [*Mourgues and Cobbold*, 2006a, 2006b; *Mourgues et al*., 2009]. Figure 5c shows calculations of the basal fluid overpressure ratio for various values of the ratio H′/H. Though fluid overpressure was not strictly constant ($\lambda^*_b = 0.23 \pm 0.04$ in the case illustrated in Figures 5b and 5c), a value of 0.75 of the ratio H′/H allowed us to minimize variations in λ^*_b (Figure 5c) along the detachment surface.

The basal fluid pressure was increased until sliding of the cover was triggered. The critical pressure required for sliding of the wedge to be initiated was then measured and the basal fluid overpressure ratio (λ^*_b) determined. To verify our analytical predictions, we tested various combinations of basal dip and surface slope angle. These verifications only focused on massive gravitational instabilities rooting in the detachment layer (i.e., the glass microbeads). Investigations on the triggering of shallow destabilizations (i.e., rooting within the sand wedge) would have required the surface slope angle to be increased as the basal fluid pressure remained constant during the experiment.

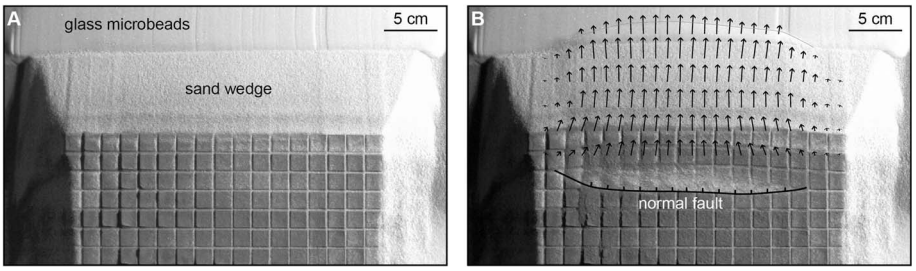

Figure 6. Top views of the downslope edge of the model, (a) before and (b) after landslide triggering. Arrows indicate surface displacements calculated from image cross correlation [*Pons and Mourgues*, 2012].

©2013. American Geophysical Union. All Rights Reserved.

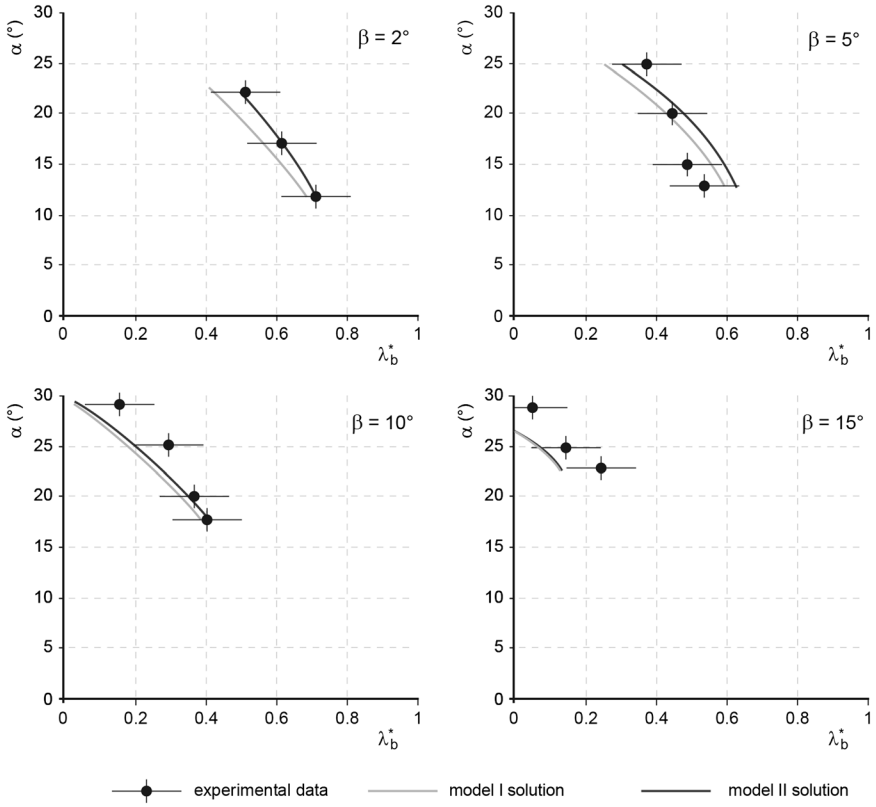

Figure 7. Experimental results (black dots) and theoretical model I (Dahlen's formulation [1984]) (grey solid lines) and model II (this study, black solid lines) predictions. The theoretical predictions take into account the dependency of λ^* on λ_b^* in the sand models.

4.2. Results

As observed by *Lacoste et al.* [2011, 2012], deformation initiated at the downslope edge of the models. When fluid pressure reached a critical value, a normal fault formed at the top of the downslope wedge-shaped edge of the models (Figure 6). No sand avalanche was triggered and the microbeads layer was deformed. These observations confirmed that the instability rooted on the basal detachment surface and that no shallow landslide (i.e., rooting above the detachment surface, within the sand wedge) occurred (gravity spreading area, Figure 3).

For a given geometry of the wedge, the coefficient of fluid pressure required to trigger sliding decreases with the basal slope (β) increasing (Figure 7). For a given basal slope angle, the value of the critical λ^*_b decreases as the surface slope (i.e., the taper of the wedge) increases (Figure 7). The minimal critical λ^*_b values are obtained where the surface slope angle reaches values close to the angle of internal friction of the sliding material ($\phi = 31°$, Table 1).

All results indicate that where the forces driving sliding are increased (i.e., where the basal and/or surface slope angle increases), the basal fluid pressure (i.e., the reduction of the basal frictional resistance) required for the critical taper to be attained diminishes. The experimental results are in good agreement with the analytical predictions of model I [*Dahlen*, 1984] and model II (this study) (Figure 7). On one hand, where $\beta = 2°$, these results are clearly in better agreement with model II. Where $\beta = 10°$and $\beta = 15°$, the experimental agreement with model II results is only slightly better than with model I. On the other hand, where $\beta = 5°$, the experimental results fit better to model I analytical curve.

5. Discussion

5.1. Comparison Between Analytical and Experimental Results

Though the observed experimental trends match the predictions, our results do not allow clear discriminations between model I and model II analytical solutions. This may be linked to experimental limitations. First, in the

©2013. American Geophysical Union. All Rights Reserved.

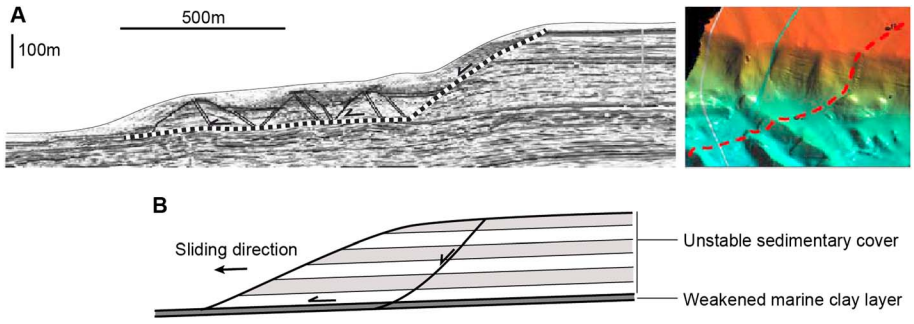

Figure 8. Geometry of the Storegga slide. (a) Interpreted seismic profile (left) and bathymetric image (right). (b) Schematic representation. Modified from *Kvalstad et al.* [2005].

theoretical analysis, the detachment is a plane, whereas it is a microbeads layer, having a given thickness, in the experiments (Figure 5a). Thus, sliding conditions vary, as the experimental normal faults may root anywhere within the overpressured microbeads layer, in which the fluid overpressure ratio decreases from bottom to top (Figure 5a). Moreover, uncertainties in the determination of λ^*_b (± 0.05) arose from the difficulties in evaluating the respective permeability of the sand and the glass microbeads. Compaction of the layers during deposition and air moisture in the experiment room may also lead to misestimating the critical fluid overpressure ratio. Furthermore, lateral air pressure losses in the models and the 3-D shape of the sliding sheet may also cause the experimental critical λ^*_b to be greater than expected.

Therefore, to justify experimentally the use of model II, low-surface slope experiments have to be carried out. Such experiments would indeed permit to verify if the evolution of the critical surface slope with the fluid overpressure ratio increase better fits to the smooth decrease in model I or to the strong reduction in model II (Figure 4). However, such modeling is very difficult to achieve because of the great basal fluid pressure required, often leading to the model blowout before any sliding event occurs.

5.2. Applicability to Natural Systems

The applicability of the results discussed above is not restricted to accretionary prisms and cover a wide range of natural settings. The presence of a weak layer acting as a décollement for the overlying cover, alongside with the absence of any downslope resistance to sliding are the sole parameters required for the model to be applied.

Therefore, such structures can be found in a variety of geological settings. For example, the critical taper theory could help better constrain the evolution of large submarine slumping, as is the case of the Storegga slide [*Kvalstad et al*., 2005], where the detachment surface is a low-resistance clay layer and where the contacts between stratigraphic layers intersect the wedge-shaped surface of the unstable mass (i.e., where no downslope buttress is found; Figure 8). Mass transport deposits occurring along passive margins subjected to fluid overpressure, as described recently by *Pattier et al.* [2011, 2013], are also a natural example where our model could be applicable. This model would also be valid for onshore landslides, such as the gravitational instabilities of the Waitawhiti complex [*Lacoste et al*., 2009].

Finally, it is important to note that the model only investigates the critical fluid pressure required to initiate sliding in the wedge. It does not allow analyses of further motion (i.e., sliding along the first formed fault and/or propagation of normal faults) that may depend on the evolution of fluid overpressure along the decollement. In natural systems, once the landslide process is initiated, fluid overpressure along the basal decollement may be reduced because of the fluid circulation along faults rooting into the detachment layer. Such a behavior is not predicted by the analytical model described above and cannot be experimentally simulated. Indeed, though the use of compressed air in our experiments allows for the reproducing of fluid overpressure distribution within the wedge, the fluid flows are not scaled (see discussion in *Mourgues and Cobbold* [2006b]). Experiments involving a more viscous fluid and less permeable materials would be necessary to investigate the further evolution of the slide and fault dynamics.

©2013. American Geophysical Union. All Rights Reserved.

6. Conclusions

We adapted the critical Coulomb wedge theory to the study of wedge-shaped masses subjected to gravitational instabilities. We derived an expression of the critical value of the basal pore pressure ratio (λ^*_b) required for the system to deform.

1. Where λ^*_b does not reach its critical value, no deformation occurs. Otherwise, two kinds of gravitational deformation may affect the system: shallow slumping and/or deep gravitational spreading rooting on the basal detachment.
2. Below a threshold value of λ^*_b, the basal detachment is not active and deformation is predicted to be restricted to shallow slumping when the surface slope of the wedge is greater than a critical value, depending on the pore pressure within the wedge (λ^*).
3. For critical fluid overpressure ratios greater than the threshold value, gravitational spreading, potentially combined with shallow slumping, is predicted to be triggered. The critical fluid overpressure ratio value increases with the angle of the surface slope decreasing.

We performed analogue experiments involving pore fluid overpressure to verify these predictions. The results are in good agreement with the theory. However, more experiments are required, as well as comparisons with natural examples, such as passive margins destabilizations.

Appendix A: Determination of σ'_{xx} Within the Wedge

In a uniform and noncohesive wedge, the orientations of stresses do not vary from place to place. σ'_{zz} and σ'_{xz} are determined from the static equilibrium of effective stresses and from the boundary conditions on the upper surface of the wedge and are given by equations (3a) and (3b). σ'_{xx} remains indefinite, and it requires additional hypotheses on the rheology of the wedge. Assuming a wedge on the verge of failure everywhere, two distinct solutions can be found (Figure A1). These solutions can be plotted in Mohr diagrams as two circles (compressive and extensive state of stress corresponding respectively to the "passive" and "active" states in Rankine's Earth pressure theory) [*Terzaghi*, 1943]. We only used solutions (1a) and (1b) in this study. From geometrical considerations, the σ'_{xx} solutions can be found by expressing the radius (r) of the Mohr circle in two ways:

1.

$$\text{In triangle } O\text{-}B\text{-}\sigma'_o : r = \sigma'_o \sin\phi \tag{A1}$$

2.

$$\text{In triangle } \sigma'_o\text{-}A\text{-}\sigma'_{zz} : r = \sqrt{\left(\sigma'^{\,2}_{xz} + (\sigma'_{zz} - \sigma'_o)^2\right)} \tag{A2}$$

with σ'_o the center of the circle.

By equalizing these two expressions, a second order equation is found

$$\sigma'^{\,2}_o \cos^2\phi - 2\sigma'_{zz}\sigma'_o + \sigma'_{xz} + \sigma'_{zz} = 0 \tag{A3}$$

After some manipulations, the discriminant Δ can be written

$$\Delta = 4\sigma'^{\,2}_{zz} \sin^2\phi\left(1 - \mathrm{FS}^2\right) \tag{A4}$$

And two distinct values of σ_o are found

$$\sigma'_o = \sigma'_{zz}\frac{1 \pm \sin(\phi)\sqrt{1 - \mathrm{FS}^2}}{\cos^2(\phi)} \tag{A5}$$

Solutions (5), (6a), and (6b) are then deduced from $\sigma'_{xx} = 2\sigma'_o - \sigma'_{zz}$.

Appendix B: Change of Coordinate System

The normal stress (σ'_n) and the shear stress (τ) acting on the detachment of the wedge are deduced from σ'_{xx}, σ'_{xz} and σ'_{zz} by a rotation of Cartesian coordinates (Figure 2). In the new coordinate system (x_1,z_1), σ'_{z1z1} (= σ'_n), and σ'_{x1z1} (= τ) are deduced from

©2013. American Geophysical Union. All Rights Reserved.

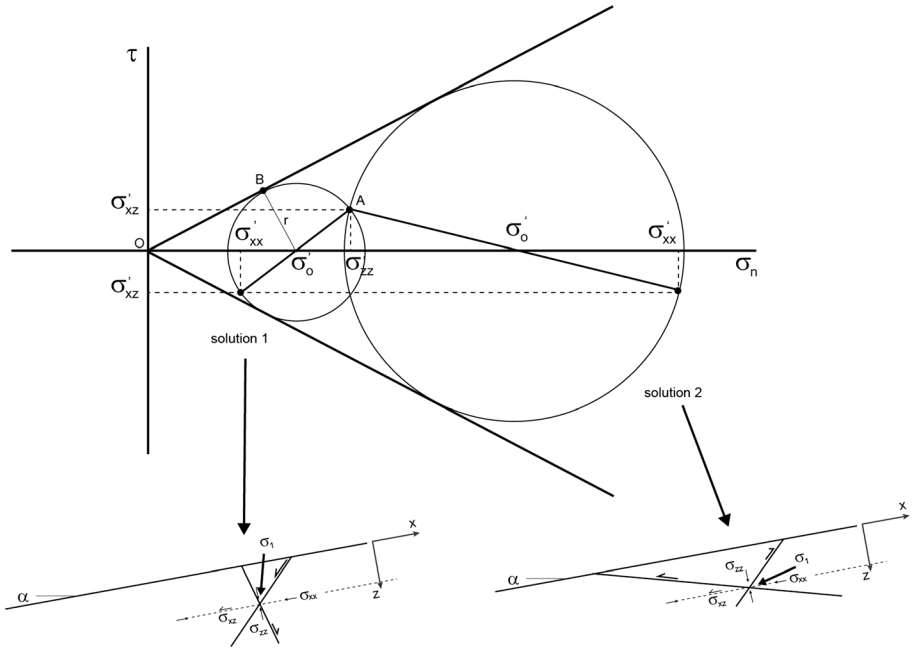

Figure A1. Graphical determination of σ'_{xx} using Mohr circles. In this study, we used solutions 1a and 1b.

$$\sigma'_{z_1z_1} = \frac{\sigma'_{xx} + \sigma'_{zz}}{2} - \frac{\sigma'_{xx} - \sigma'_{zz}}{2}\cos(2(\alpha - \beta)) - \sigma'_{xz}\sin(2(\alpha - \beta)) \quad \text{(B1)}$$

$$\sigma'_{x_1z_1} = \frac{\sigma'_{xx} - \sigma'_{zz}}{2}\sin(2(\alpha - \beta)) + \sigma'_{xz}\cos(2(\alpha - \beta)) \quad \text{(B2)}$$

Acknowledgments
We are grateful to Fabien Graveleau and an anonymous reviewer for their comments that contributed to improve the present manuscript.

References

Bilotti, F., and J. Shaw (2005), Deep-water Niger Delta fold and thrust belt modelled as a critical taper wedge: The influence of elevated basal fluid pressure on structural styles, *Am. Assoc. Pet. Geol. Bull.*, *89*, 1475–1491.
Bishop, A. W. (1955), The use of the slip circle in the stability analysis of slopes, *Geotechnique*, *5*, 7–17.
Dahlen, F. (1984), Noncohesive critical coulomb wedges: An exact solution, *J. Geophys. Res.*, *89*(B12), 10,125–10,133.
Dahlen, F. (1990), Critical taper model of fold-and-thrust belts and accretionary wedges, *Annu. Rev. Earth Planet. Sci.*, *18*(1), 55–99.
Dahlen, F., J. Suppe, and D. Davis (1984), Mechanics of fold-and-thrust belts and accretionary wedges: Cohesive Coulomb theory, *J. Geophys. Res.*, *89*(B12), 10,087–10,101.
Davis, D., J. Suppe, and F. A. Dahlen (1983), Mechanics of fold-and-thrust belts and accretionary wedges, *J. Geophys. Res.*, *88*(B2), 1153–1172.
Gutscher, M. A., N. Kukowski, J. Malavieille, and S. Lallemand (1998), Material transfer in accretionary wedges from analysis of a systematic series of analog experiments, *J. Struct. Geol.*, *20*, 407–416.
Hubbert, M. K., and W. W. Rubey (1959), Role of fluid pressure in mechanics of overthrust faulting, *Geol. Soc. Am. Bull.*, *70*, 115–166.
Hutton, E. W. H., and J. P. M. Syvitski (2004), Advances in the numerical modeling of sediment failure during the development of a continental margin, *Mar. Geol.*, *203*, 367–380.
Jaeger, J. C., and N. G. W. Cook (1979), *Fundamentals of Rock Mechanics*, 3rd ed., Chapman and Hall, London, U.K.
Kopf, A., and K. M. Brown (2003), Friction experiments on saturated sediments and their implications for the stress state of the Nankai and Barbados subduction thrusts, *Mar. Geol.*, *202*, 193–210.
Kukowski, N., T. Schillhorn, K. Huhn, U. von Rad, S. Husen, and E. R. Flueh (2001), Morphotectonics and mechanics of the Central Makran accretionary wedge off Pakistan, *Mar. Geol.*, *173*, 1–19.
Kukowski, N., J. Greinert, and S. Henrys (2010), Morphometric and critical taper analysis of the Rock Garden region, Hikurangi Margin, New Zealand: Implications for slope stability and potential tsunami generation, *Mar. Geol.*, *272*, 141–153.
Kvalstad, T. J., L. Andresen, C. F. Forsberg, K. Berg, P. Bryn, and M. Wangen (2005), The Storegga Slide: Evaluation of triggering sources and slide mechanisms, *Mar. Pet. Geol.*, *22*, 245–256.
Lacoste, A., L. Loncke, F. Chanier, J. Bailleul, B. C. Vendeville, and G. Mahieux (2009), Morphology and structure of a landslide complex in an active margin setting: The Waitawhiti complex, North Island, New Zealand, *Geomorphology*, *109*, 184–196.
Lacoste, A., B. C. Vendeville, and L. Loncke (2011), Influence of combined incision and fluid overpressure on slope stability: Experimental modelling and natural applications, *J. Struct. Geol.*, *33*, 731–742.
Lacoste, A., B. C. Vendeville, R. Mourgues, L. Loncke, and M. Lebacq (2012), Gravitational instabilities triggered by fluid overpressure and downslope incision—Insights from analytical and analogue modelling, *J. Struct. Geol.*, *42*, 151–162.
Lallemand, S., P. Schnürle, and J. Malavieille (1994), Coulomb theory applied to accretionary and nonaccretionary wedges: Possible causes for tectonic erosion and/or frontal accretion, *J. Geophys. Res.*, *99*(B6), 12,033–12,055.
Lambe, T. W., and R. V. Whitman (1969), *Soil Mechanics*, Wiley, New York.
Lehner, F. K. (1986), Comments on "noncohesive critical Coulomb wedges: An exact solution" by F.A. Dahlen, *J. Geophys. Res.*, *91*(B1), 793–796.

©2013. American Geophysical Union. All Rights Reserved.

Leynaud, D., J. Mienert, and F. Nadim (2004), Slope stability assessment of the Helland Hansen area offshore the mid-Norwegian margin, *Mar. Geol.*, *213*, 454–480.
Martinez, A., J. Malavieille, S. Lallemand, and J.-Y. Collot (2002), Partition de la déformation dans un prisme d'accrétion sédimentaire en convergence oblique: Approche expérimentale, *Bull. Soc. Geol. Fr.*, *173*, 17–24.
Mello, U. T., and L. F. Pratson (1999), Regional slope stability and slope-failure mechanics from the two-dimensional state of stress in an infinite slope, *Mar. Geol.*, *154*, 339–356.
Morgan, J. K., and P. J. McGovern (2005), Discrete element simulations of gravitational volcanic deformation: 2. Mechanical analysis, *J. Geophys. Res.*, *110*, B05403, doi:10.1029/2004JB003253.
Morley, C. K., R. King, R. Hillis, M. Tingay, and G. Backe (2011), Deepwater fold and thrust belt classification, tectonics, structure and hydrocarbon prospectivity: A review, *Earth Sci. Rev.*, *104*, 41–91.
Mourgues, R., and P. R. Cobbold (2003), Some tectonic consequences of fluid overpressures and seepage forces as demonstrated by sandbox modeling, *Tectonophysics*, *376*, 75–97.
Mourgues, R., and P. R. Cobbold (2006a), Sandbox experiments on gravitational spreading and gliding in the presence of fluid overpressures, *J. Struct. Geol.*, *28*, 887–901.
Mourgues, R., and P. R. Cobbold (2006b), Thrust wedges and fluid overpressures: Sandbox models involving pore fluids, *J. Geophys. Res.*, *111*, B05404, doi:10.1029/2004JB003441.
Mourgues, R., E. Lecomte, B. Vendeville, and S. Raillard (2009), An experimental investigation of gravity-driven shale tectonics in progradational delta, *Tectonophysics*, *474*, 643–656.
Mulugeta, G. (1988), Modelling the geometry of Coulomb thrust wedges, *J. Struct. Geol.*, *10*, 847–859.
Nadim, F., D. Krunic, and P. Jeanjean (2003), Probabilistic slope stability analyses of the Sigsbee Escarpment, Proceedings, OTC paper 15203, paper presented at Offshore Technology Conference, Houston, Tex., pp. 1–8.
Osborne, M. J., and R. E. Swarbrick (1997), Mechanisms for generating overpressure in sedimentary basins: A reevaluation, *Am. Assoc. Pet. Geol. Bull.*, *81*, 1023–1041.
Pattier, F., L. Loncke, V. Gaullier, B. Vendeville, A. Maillard, C. Basile, M. Patriat, W. R. Roest, and B. Loubrieu (2011), Mass movements in a transform margin setting: The example of the Eastern Demerara Rise, in *Submarine Mass Movements and Their Consequences*, Advances in Natural and Technological Hazards Research, vol. 31, edited by Y. Yamada et al., pp. 331–339, Springer, Berlin, Germany.
Pattier, F., L. Loncke, C. Basile, A. Maillard, P. Imbert, W. R. Roest, B. C. Vendeville, M. Patriat, and B. Loubrieu (2013), Mass-transport deposits and fluid venting in a transform margin setting, the eastern Demerara Plateau (French Guiana), *Mar. Pet. Geol.*, *46*, 287–303.
Platt, J. P. (1986), Dynamics of orogenic wedges and the uplift of high-pressure metamorphic rocks, *Geol. Soc. Am. Bull.*, *97*, 1037–1053.
Pons, A., and R. Mourgues (2012), Deformation and stability of over-pressured wedges—Insight from sandbox models, *J. Geophys. Res.*, *117*, B09404, doi:10.1029/2012JB009379.
Reis, A. T., R. Perovano, C. G. Silva, B. C. Vendeville, E. Araujo, C. Gorini, and V. Oliveira (2010), Two-scale gravitational collapse in the Amazon Fan: A coupled system of gravity tectonics and mass-transport processes, *J. Geol. Soc. London*, *167*, 593–604.
Saffer, D. M., and B. A. Bekins (1998), Episodic fluid flow in the Nankai accretionary complex: Timescale, geochemistry, flow rates, and fluid budget, *J. Geophys. Res.*, *103*(B12), 30,351–30,370.
Schellart, W. P. (2000), Shear test results for cohesion and friction coefficients for different granular materials: Scaling implications for their usage in analogue modelling, *Tectonophysics*, *324*, 1–16.
Shi, Y., and C. Wang (1988), Generation of high pore pressures in accretionary prisms: Inferences from the Barbados subduction complex, *J. Geophys. Res.*, *93*(B8), 8893–8909.
Simpson, G. (2011), Mechanics of non-critical fold–thrust belts based on finite element models, *Tectonophysics*, *499*, 142–155.
Suppe, J. (1981), Mechanics of mountain building and metamorphism in Taiwan, *Mem. Geol. Soc. China*, *4*, 67–89.
Suppe, J. (2007), Absolute fault and crustal strength from wedge tapers, *Geology*, *35*, 1127–1130.
Terzaghi, K. (1943), *Theoretical Soil Mechanics*, Wiley, New York.
Terzaghi, K.v. (1923), Die berechnung der durchlässigkeitsziffer des tones aus dem verlauf der hydrodynamischen spannungerscheinungen, *Akad. Wissensch. Wien., Math. Naturw. KL. Abt*, *132*, 125–138.
Wang, K., J. He, and Y. Hu (2006), A note on pore fluid pressure ratios in the Coulomb wedge theory, *Geophys. Res. Lett.*, *33*, L19310, doi:10.1029/2006GL027233.
Willett, S. D. (1992), Dynamic and kinematic growth and change of a Coulomb wedge, in *Thrust Tectonics*, edited by K. R. McClay, pp. 19–31, Chapman and Hall, London, U.K.
Xiao, H.-B., F. A. Dahlen, and J. Suppe (1991), Mechanics of extensional wedges, *J. Geophys. Res.*, *96*(B6), 10,301–10,318.
Zhao, W.-L., D. M. Davis, F. A. Dahlen, and J. Suppe (1986), Origin of convex accretionary wedges: Evidence from Barbados, *J. Geophys. Res.*, *91*(B10), 10,246–10,258.

©2013. American Geophysical Union. All Rights Reserved.